

A 206-GHz Transformer-Based Super-Regenerative Oscillator with up to 39 dB Gain and 15 GHz Switching Rate in 130-nm SiGe BiCMOS

Yu Zhu^{#1}, Tilo Meister^{#2}, Frank Ellinger^{#3}

[#]Chair for Circuit Design and Network Theory, Technische Universität Dresden, Germany
 {¹yu.zhu2, ²tilo.meister, ³frank.ellinger}@tu-dresden.de

Abstract—This paper investigates a super-regenerative oscillator (SRO) operating at 206 GHz that is based on a differential common-collector Colpitts oscillator topology and transformer. The SRO is used to regenerate a very small input signal into a substantially larger output signal by recovering its phase. An input stage utilizing an on-chip transformer is designed to feed the input signal to the differential oscillator. To prove the concept, the circuit is fabricated in a 130-nm BiCMOS technology with a total chip area of 0.88 mm². Measurement results demonstrate a minimum input sensitivity of -47 dBm for a phase-coherent output. The oscillator has a maximum output power of -3 dBm and achieves a maximum regenerative gain of 39 dB. A frequency tuning range of 3.6% from 204.2 GHz to 211.6 GHz has been realized. Furthermore, the circuit requires a dc power of only 12.4 mW leading to a DC-to-RF power efficiency of 4%. This work achieves a maximum quenching frequency of 15 GHz. Compared to the state of the art, this is the SRO with the fastest quenching frequency reported to date.

Index Terms—Super-regenerative oscillator, millimeter wave integrated circuits, THz receiver, high-resolution imaging.

I. INTRODUCTION

Lately, due to the exceptional wave properties and a wide range of potential applications, the interest in the terahertz (THz) region (100 GHz–10000 GHz) has rapidly increased. Unlike microwave signals, they allow for very high-resolution imaging, thanks to their short wavelength. In order to leverage the potential benefits of THz imaging for real-world practical applications, power efficient, highly sensitive and compact THz imaging systems with multichannel signal acquisition are needed. At THz frequencies, to compensate the very high free space path loss, an amplifier with a very high gain for imaging systems is required. However, the imaging system architectures based on conventional heterodyne transceivers suffer from low gain, high power consumption, high noise, large chip area and high heat dissipation, when transistors operate close to or beyond the maximum oscillation frequency (f_{\max}) of the transistors.

In order to solve these fundamental shortcomings for THz camera receivers, the super-regenerative receivers (SRR) system concept based on using a super-regenerative oscillator (SRO) for amplification becomes increasingly attractive for efficient signal reception [1], [2]. The SRO is based on an amplifier requiring only low small-signal gain. This amplifier is connected in a positive feedback loop from the output to the

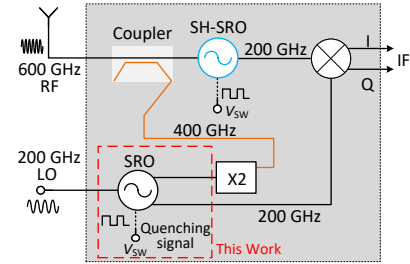


Fig. 1. Block diagram of the complete super-regenerative receiver, including the auxiliary SRO and a quadrature down-conversion mixer.

input, leading to a high large-signal gain due to the constructive feedback. Therefore, the SRR provides the big advantages of achieving a high gain and a high sensitivity at a low complexity, size, cost and power consumption. The block diagram of the proposed receiver is shown in Fig. 1. Using a novel subharmonic-pumped SRO concept, the received 600 GHz signal is down-converted to an intermediate frequency (IF) of 200 GHz using a pulsed local oscillator combined with a high super-regenerative amplification utilizing positive feedback. The feasibility of such mixing products has already been shown for intermodulation with an incoherent second oscillator with 2nd harmonic downconversion [3], which can be extended to 3rd harmonic operation and full coherence. To ensure coherent regeneration, an auxiliary SRO and a frequency doubler are implemented for coherent LO regeneration from its signal distribution network. In addition, SRO-based LO regeneration also allows for elegant compensation of unequal insertion loss in the feed network. In this proof-of-concept study, such an auxiliary SRO is investigated.

II. DESIGN AND IMPLEMENTATION OF THE SRO

The circuit schematic of the proposed transformer-based SRO is illustrated in Fig. 2. It comprises three main blocks: an oscillator core, an injection stage and a quenching stage. Due to the good performance of the differential common-collector Colpitts topology at high frequencies [4], it is chosen for the oscillator core design. The oscillator core is realized with transistors $T_{7,8}$ and a LC resonator, which is composed of the transmission lines TL_{res} and the base-collector diodes using transistor pair $T_{5,6}$ as varactors. Thus, the frequency tuning is achieved by adjusting the voltage V_{tune} , which cor-

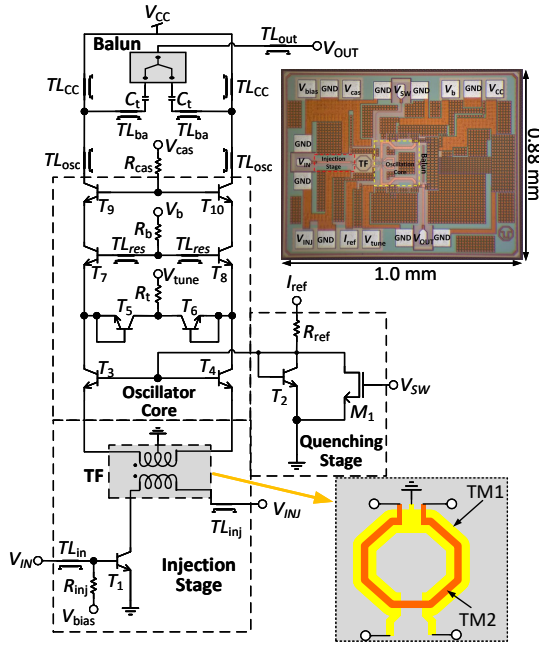


Fig. 2. Schematic and chip micrograph of the 206 GHz SRO with pad labels.

responds to varying the base-collector voltage of varactors. A differential common-base output buffer comprising transistors $T_{9,10}$ is implemented to deliver maximum output power to the load, since it provides the required low impedances at the collectors of $T_{7,8}$ and allows to drive a high-impedance load. Additionally, it offers sufficient reverse isolation to prevent the oscillator from locking on the reflected pulses, when the output impedance appears mismatch. To obtain optimal load impedances, the output matching network, which consists of transmission lines TL_{osc} , TL_{CC} , TL_{ba} , and a metal-insulator-metal (MIM) capacitor C_t , were implemented by means of the load-pull simulations. Simultaneously, the fast start-up time has to be taken into account regarding load-pull simulations, to enable a pulsed operation of the SRO with a fast quenching above 10 GHz. Therefore, a trade-off value was chosen as the optimum load impedance between a higher steady-state oscillation output amplitude and a faster start-up time. To facilitate differential-to-single-ended signal conversion at the output interface, a three-conductor T-Line balun proposed in [5] has been implemented, which simplifies the measurement setup and also achieves the impedance transformation to a single-ended 50Ω load.

For the injection of an input signal into the oscillator, an injection stage composed of a common-emitter buffer with transistor T_1 and an on-chip transformer is employed. Consequently, it behaves as an active balun to feed the single-ended input signal to the differential input of the oscillator. The common-emitter buffer is implemented to provide optimal 50Ω impedance matching while delivering preliminary input signal amplification. The transformer is designed using two stacked lines in the top two metal layers, the supply voltage V_{INJ} is provided through the line in the topmost layer. Utilizing an on-chip transformer results in independent biases of the

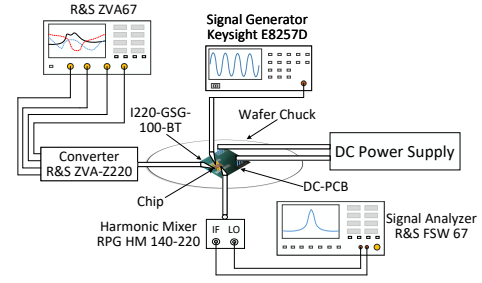


Fig. 3. Experimental setup for on-wafer probing of the fabricated circuit.

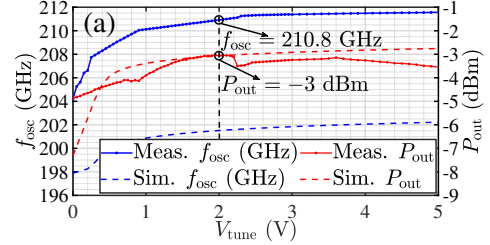


Fig. 4. Measured (solid lines) and simulated (dashed lines) oscillation frequency (left) and output power (right) versus the varactor tuning voltage V_{tune} of the SRO at the free running mode.

input buffer and the oscillator, which realizes more efficient input signal recovering. This helps to save headroom for the oscillator, since the input stage is coupled to the oscillator through the transformer instead of stacking the oscillator on top of T_1 . Therefore, the SRO can operate at lower supply voltage V_{CC} and dc power, and thus a larger output swing is obtained for a given supply. By means of impedance conversion of the transformer, a much lower impedance can be obtained at the emitter nodes of the $T_{7,8}$, which leads to a reduced emitter degeneration impedance. Thus, the regenerative gain of the proposed SRO has been maximized. Simultaneously, the parasitic capacitance between the base of the tail transistor and ground can be reduced due to the impedance transformation, which results in a lower switching time constant and thus achieves a higher switching rate.

To sample the phase and amplitude information of the input signal at the turn-on instant, the oscillator has to be periodically quenched, thus each oscillation pulse represents one symbol. The quenching of the SRO is performed by transistors T_3 and T_4 , which form a current mirror with a diode-connected transistor T_2 for the oscillator core. Thus, the current biasing is set through I_{ref} . The switching signal is applied to periodically quench the oscillator as desired using a nMOS transistor M_1 , whose drain is connected to the base of the current mirror, by driving down the bias voltage node to turn off the current mirror during the off phase.

III. EXPERIMENTAL RESULTS

To prove and investigate the concept, the circuit was implemented in a 130-nm SiGe BiCMOS technology, which has an f_T/f_{max} of 470 GHz/650 GHz. The key characteristics of the HBT technology are described in [6]. The chip micrograph is presented in Fig. 2. The total chip occupies an area of 0.88 mm^2 including chip pads. The total dc power is 22.4 mW

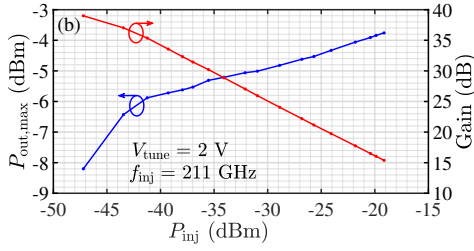


Fig. 5. Measured maximum output spectral power $P_{out,max}$ (left) and the corresponding regenerative gain (right) versus the input power P_{inj} for an input frequency f_{inj} of 211 GHz.

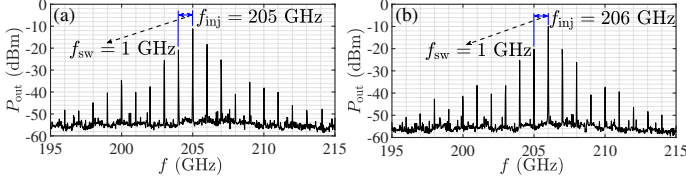


Fig. 6. Measured spectrum for quench frequency of $f_{sw}=1$ GHz at oscillation frequency of $f_{osc} \approx 205.5$ GHz, with (a) $P_{inj} = -24.5$ dBm at $f_{inj} = 205$ GHz (b) $P_{inj} = -26$ dBm at $f_{inj} = 206$ GHz.

under two supplies of $V_{CC}=3.3$ V and $V_{INJ}=1$ V, when the circuit operates in free-running mode, i.e. without input signal. All on-chip dc power distribution networks are realized through zero-Ohm transmission lines, which ensure effective ac grounding and achieve high power delivery efficiency [4]. Furthermore, while the SRO is being quenched at a duty cycle of 50%, the dc power reduces to 12.4 mW. To characterize the implemented circuit on-wafer, its dc pads have been wire-bonded on a custom printed circuit board (PCB). However, due to the high operation frequency, which is beyond the range of available oscilloscopes, time-domain measurements cannot be directly performed. Therefore, the circuit can only be characterized in the frequency-domain. The measurement setup is sketched in Fig. 3. To generate a continuous wave (CW) input signal between 140 GHz – 220 GHz, a Rohde&Schwarz ZVA-Z220 network analyzer converter was used. In order to measure the spectrum, the output of the SRO circuit was connected to a Radiometer Physics HM140-220 harmonic mixer, which is combined with a Rohde&Schwarz FSW67 signal analyzer. A Keysight E8257D signal generator provided V_{sw} , the quenching signal for SRO operation. In addition, a Virginia Diodes PM4 power meter is used for power calibrations and signal power measurements.

In order to verify the regenerative phase sampling capability of the SRO, the measured output spectrum of a phase-locked SRO is derived in [7], [8] as

$$V_{out}(f) = A_{out} D_{sw} \left| \text{sinc}(\pi T_{on}(f - f_{osc})) \right| \cdot \sum_{n=-\infty}^{\infty} \delta((f - f_{inj}) - n f_{sw}) \quad (1)$$

where A_{out} is the output amplitude, $D_{sw}=T_{on} \cdot f_{sw}$ is the duty cycle of the switching signal, T_{on} and f_{sw} are the period of the oscillator on-state before quenching and the switching frequency, respectively. Equation (1) shows that the output spectrum $V_{out}(f)$ has a sequence of Dirac impulses

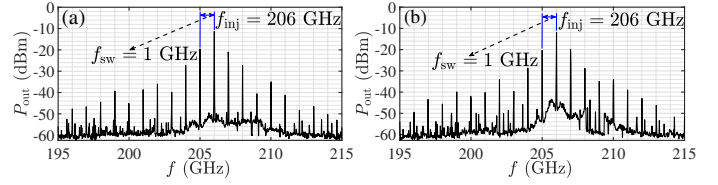


Fig. 7. Measured spectrum for quench frequency of $f_{sw}=1$ GHz and input frequency of $f_{inj}=206$ GHz at oscillation frequency of $f_{osc} \approx 205.5$ GHz, with (a) $P_{inj} = -37.4$ dBm (b) $P_{inj} = -47$ dBm.

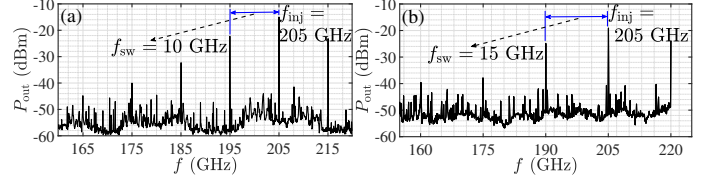


Fig. 8. Measured spectrum for input frequency of $f_{inj}=205$ GHz and input power of $P_{inj} = -35.3$ dBm at oscillation frequency of $f_{osc} \approx 205.5$ GHz, with (a) $f_{sw}=10$ GHz (b) $f_{sw}=15$ GHz.

at $f_{inj} - n f_{sw}$, where f_{inj} is the injection frequency and n is an integer, and these spectral components are centered at the oscillation frequency f_{osc} and have a sinc-shaped envelope. Thus, every two adjacent spectral components have a certain distance which equals the switching frequency.

Fig. 4 shows the measured and simulated oscillation frequency f_{osc} and output power P_{out} of the SRO as a function of the varactor tuning voltage V_{tune} at its free running mode, as both the SRO input signal (V_{IN}) and the quenching signal (V_{sw}) input are terminated to 50 Ω . The measured f_{osc} can be tuned between 204.2 GHz and 211.6 GHz by V_{tune} from 0 V to 5 V, which corresponds to a tuning range of 3.6%. A maximum output power of -3 dBm at 210.8 GHz is provided in its free running operation. Moreover, the output power measurements align closely with the simulations, although the measured oscillation frequencies are slightly higher than the simulations. For the injection locking condition, Fig. 5 presents the maximum spectral power $P_{out,max}$ versus the input power P_{inj} . As a result, the maximum regenerative gain is 39 dB, with a sensitivity as low as -47 dBm.

To characterize the phase-sampling functionality of the SRO, its output spectrum is illustrated in Fig. 6, when the quench and oscillation frequencies are set to 1 GHz and 205.5 GHz, respectively. Due to the duty cycle of 50%, dc power drops to 12.4 mW. Fig. 6(a) shows the measured output spectrum for an input CW signal at 205 GHz with a power level of -24.5 dBm, it can be observed that the spectral envelope is centered around f_{osc} and all spectral components follow the f_{inj} , and each two adjacent spectral components have the exact distance of integer multiples of the switching frequency ($n f_{sw}$), as described by (1). In Fig. 6(b), the identical result is confirmed, although an input CW signal at 206 GHz with an input power of -26 dBm has been chosen. Decreasing the input power level of f_{inj} at 206 GHz to -37.4 dBm and -47 dBm, as shown in Fig. 7(a) and (b), respectively. In Fig. 7(b), due to recognizable spectral components, the phase-coherence has

TABLE I
COMPARISON OF STATE-OF-THE-ART MM-WAVE SROS.

Ref.	This work	[9]	[7]	[8]	[10]	[11]	[12]	[13]	[14]	[4]
Technology	130 nm SiGe	65 nm CMOS	250 nm SiGe	22 nm FD-SOI	130 nm SiGe	130 nm SiGe	65 nm CMOS	65 nm CMOS	130 nm SiGe	130 nm SiGe
f_{\max} (GHz)	650	N.A.	180	371	450	450	N.A.	N.A.	450	450
f_{osc} (GHz)	206	144	34.5	60	61.5	60	130	183	160	180
P_{out} (dBm)	-3	-33.5 [^]	5	1.5	4.5	3.1	-13.5	N.A.	-8.4	0.5
P_{DC} (mW)	12.4[†]	2.5	122 [†]	10 [§]	13 [~]	25 [#]	8.1 [†]	13.5 [†]	6.6 [†]	8.8 [#]
$P_{\text{out}}/P_{\text{DC}}$ (%)	4	0.018	2.6	14.1	21.7	8.16	0.55	N.A.	2.2	12.8
Tuning range (%)	3.6	N.A.	8	10	12	11.7*	2.7	N.A.	N.A.	6.5
$P_{\text{inj,min}}$ (dBm)	-47	-74	-61.5	-42	-40	-79.5	-84	-72.5	-27	-58
f_{sw} (MHz)	15000	10	75	10000	3000	10	12	150	5000	10000
$f_{\text{sw}}/f_{\text{osc}}$ (%)	7.28	0.007	0.2	16.7	4.9	0.017	0.009	0.08	3.1	5.6
Area (mm ²)	0.88	0.3	0.83	0.49	0.96	0.87	0.3	N.A.	0.64	0.72

[^]: calculated from plot, ^{*}: graphically estimated, [§]: duty cycle=55%, [†]: duty cycle=50%, [#]: duty cycle=30%, [~]: duty cycle=15%.

been verified even for a minimum $P_{\text{inj}}=-47$ dBm. Compared to Fig. 7(a) that higher $P_{\text{inj}}=-37.4$ dBm causes a better phase-sampling functionality and reduced sampling errors, as the noise floor around the center frequency is lower. Additionally, switching rates of 10 GHz and 15 GHz with an input power of -35.3 dBm are shown in Fig. 8(a) and (b), respectively. The implemented SRO exhibits a peak switching frequency reaching 15 GHz.

IV. CONCLUSION

This paper investigates an SRO circuit operating at 206 GHz that utilizes a differential common-collector Colpitts oscillator configuration. For the high-resolution THz imaging application, the SRO is utilized as a main circuit block in a super-regenerative receiver system, to regenerate a very small input signal into a significantly large output signal by restoring its phase. An injection stage employing an on-chip transformer is presented to deliver a differential input signal to the oscillator. As a result of adopting the transformer, the regenerative gain and switching rate were improved, due to reduced emitter degeneration and lower parasitic capacitance at the base of the tail transistor. The measurements of the SRO demonstrate a minimum input signal power of -47 dBm with a regenerative gain of 39 dB, and a maximum output power of -3 dBm. Only a dc power of 12.4 mW was needed for the SRO operating in pulsed mode, thus a DC-to-RF efficiency of 4% has been achieved. The SRO exhibits a frequency tuning range of 3.6%, from 204.2 GHz to 211.6 GHz. In Table I, the proposed SRO is compared against the other state of the art mm-wave SROS. This SRO presents the fastest switching rate of 15 GHz, which is, to the best knowledge of the authors, the fastest reported by far.

ACKNOWLEDGMENT

This research was supported by the German Research Foundation (DFG) within the frame of the projects ‘‘TeraCaT’’ (under grant 506/45-1) and ‘‘TeraCaT II’’ (under grant 506/45-2).

REFERENCES

[1] C. Carlowitz and M. Vossiek, ‘‘Concept for a novel low-complexity qam transceiver architecture suitable for operation close to transition frequency,’’ in *2015 IEEE MTT-S International Microwave Symposium*, 2015, pp. 1–4.

[2] C. Carlowitz and M. Vossiek, ‘‘Demonstration of an efficient high speed communication link based on regenerative sampling,’’ in *2017 IEEE MTT-S International Microwave Symposium (IMS)*, 2017, pp. 71–74.

[3] A. Tang and M.-C. F. Chang, ‘‘Inter-Modulated Regenerative CMOS Receivers Operating at 349 and 495 GHz for THz Imaging Applications,’’ *IEEE Transactions on Terahertz Science and Technology*, vol. 3, no. 2, pp. 134–140, 2013.

[4] H. Ghaleb, C. Carlowitz, D. Fritsche, P. Starke, F. Protze, C. Carta, and F. Ellinger, ‘‘A 180-GHz Super-Regenerative Oscillator With up to 58 dB Gain for Efficient Phase and Amplitude Recovery,’’ *IEEE Transactions on Microwave Theory and Techniques*, vol. 68, no. 6, pp. 2011–2019, 2020.

[5] Y. Zhu, T. Meister, and F. Ellinger, ‘‘Design and Characterization of a Compact and Broadband On-Chip Modified Three-Conductor Transmission Line Balun at G-Band,’’ in *2025 IEEE Wireless and Microwave Technology Conference (WAMICON)*, 2025, pp. 1–4.

[6] H. Rucker and B. Heinemann, ‘‘Device Architectures for High-speed SiGe HBTs,’’ in *2019 IEEE BiCMOS and Compound semiconductor Integrated Circuits and Technology Symposium (BCICTS)*, 2019, pp. 1–7.

[7] A. Strobel, C. Carlowitz, R. Wolf, F. Ellinger, and M. Vossiek, ‘‘A Millimeter-Wave Low-Power Active Backscatter Tag for FMCW Radar Systems,’’ *IEEE Transactions on Microwave Theory and Techniques*, vol. 61, no. 5, pp. 1964–1972, 2013.

[8] A. Ferschischi, H. Ghaleb, Z. Tibenszky, C. Carta, and F. Ellinger, ‘‘A Power Efficient 60-GHz Super-Regenerative Oscillator with 10-GHz Switching Rate in 22-nm FD-SOI CMOS,’’ in *2020 IEEE/MTT-S International Microwave Symposium (IMS)*, 2020, pp. 349–352.

[9] A. Tang, Z. Xu, Q. J. Gu, Y.-C. Wu, and M. C. F. Chang, ‘‘A 144 GHz 2.5mW multi-stage regenerative receiver for mm-Wave imaging in 65nm CMOS,’’ in *2011 IEEE Radio Frequency Integrated Circuits Symposium*, 2011, pp. 1–4.

[10] A. Ferschischi, H. Ghaleb, C. Carta, and F. Ellinger, ‘‘61.5-GHz Energy-Efficient Super-Regenerative Oscillator with Tunable Quench Duty Cycle,’’ in *2022 IEEE/MTT-S International Microwave Symposium - IMS 2022*, 2022, pp. 661–664.

[11] H. Ghaleb, N. Joram, and F. Ellinger, ‘‘A 60-GHz Super-Regenerative Oscillator with 80 dB Gain in SiGe BiCMOS for FMCW Radar Active Reflectors,’’ in *2022 IEEE 22nd Topical Meeting on Silicon Monolithic Integrated Circuits in RF Systems (SiRF)*, 2022, pp. 31–34.

[12] S. Ma, H. Yu, Q. J. Gu, and J. Ren, ‘‘A 7.52-dB Noise Figure 128.75-132.25-GHz Super-Regenerative Receiver With 0.615-fW/ $\sqrt{\text{Hz}}$ NEP by Coupled Oscillator Networks for Portable Imaging System in 65-nm CMOS,’’ *IEEE Transactions on Microwave Theory and Techniques*, vol. 66, no. 9, pp. 4095–4107, 2018.

[13] A. Tang and M.-C. F. Chang, ‘‘183GHz 13.5mW/pixel CMOS regenerative receiver for mm-wave imaging applications,’’ in *2011 IEEE International Solid-State Circuits Conference*, 2011, pp. 296–298.

[14] H. Ghaleb, P. V. Testa, S. Schumann, C. Carta, and F. Ellinger, ‘‘A 160-GHz Switched Injection-Locked Oscillator for Phase and Amplitude Regenerative Sampling,’’ *IEEE Microwave and Wireless Components Letters*, vol. 27, no. 9, pp. 821–823, 2017.